Modelling of powder hydrodynamics in a screw reactor

Lucas Chatre, Marc Bataille, Marie Debacq, Tojonirina Randriamanantea, Jeremy Nos, Florian Herbelet

Modelling of Powder Hydrodynamics in a Screw Reactor

Lucas Chatre[a,b], Marc Bataille[a], Marie Debacq[b,c], Tojonirina Randriamanantena[a], Jeremy Nos[d], Florian Herbelet[a,*]

a, CEA, DES, ISEC, DMRC, Université de Montpellier, Marcoule,
b, Université Paris-Saclay, INRAE, AgroParisTech, UMR SayFood, 91120, Palaiseau, France
c, CNAM, 2 rue Conté, 75003 Paris, France
d, ORANO Recyclage,125 Avenue de Paris, 92320, Châtillon, France
* Corresponding author. E-mail address florian.herbelet@cea.fr (F. Herbelet).

ABSTRACT

Screw reactors are largely used devices in the industry. Very few studies focus on the powder hydrodynamics in screw reactors. The overflow point, a filling degree value when the powder passes over the shaft, was determined for different conditions and a dimensionless model was fitted to predict this parameter. The residence time distribution (RTD) has been measured with a pulse injection of salty powder. The influence of operating conditions and geometry parameters on the RTD has been studied. It appeared that the Hausner ratio, the pitch length and the filling degree mostly influence the RTD shape. Two models for the RTD have been compared: the compartment model was the most accurate and has one parameter of adjustment. A dimensionless model was developed and fitted with 51 experimental RTD results, predicting the RTD shape. The dimensionless model predicts with good accuracy other experimental data from the literature.

Keywords: Screw reactor, Residence Time Distribution, Powder flowability, Modelling, Powder hydrodynamics

NOMENCLATURE

$c_1(t)$	Tracer concentration over time (g L^{-1})
c_0	Initial tracer concentration injection (g L^{-1})
D_{in}	Internal tube diameter (m)
D_{sc}	Screw diameter (m)
D_{sh}	Shaft diameter (m)
D_x	Particle diameter (with x the sample percentage having diameter less than D_x) (m)
e	Screw thickness (m)
E(t)	Probability distribution function (s^{-1})
F(t)	Cumulative distribution function (-)
$F_v(t)$	Flow rate variation curve (-)
FD	Filling degree (-)
FD_{OF}	Filling degree at the overflow point (-)
Fr	Froude number (-)
g	Gravitational acceleration (m s^{-2})

HR	Hausner ratio (-)
K	Friction coefficient (N m^{-2})
L_{sc}	Inlet-Outlet length (m)
N	Rotation speed (min^{-1})
p_{CSTR}	Continuous stirred tank reactor volume proportion (-)
p_{PFR}	Plug flow reactor volume proportion (-)
p_{sc}	Pitch length (m)
Q	Volumetric flow rate (m^3 s^{-1})
Q_m	Mass flow rate (kg s^{-1})
$Q_{m,initial}$	Initial mass flow rate (kg s^{-1})
$Q_{m,final}$	Final mass flow rate (kg s^{-1})
ρ_{bulk}	Bulk density (kg m^{-3})
s	Skewness (s^3)
$\bar{t}$	Mean residence time (s)
τ	Conveyor time of passage (s)
τ_{PFR}	Plug flow reactor time of passage (s)
θ	Static angle of repose (°)
σ^2	Signal variance (s^2)
V_{CSTR}	Continuous stirred tank reactor volume (m^3)
V_{reac}	Reactor volume (m^3)
V_{RTD}	Residence Time Distribution volume (m^3)
V_{PFR}	Plug-flow reactor volume (m^3)

1. INTRODUCTION

Screw reactors are widely found such as in the food, pharmaceutical, mining or petroleum industries [1,2]. Campuzano *et al.* give a list of pros and cons for this device [3]. One of the main advantages of this technology is its versatility in handling solid particles, with a good or poor flowability, small or big size, etc. [2,4]. Giving a good heat transfer [5,6], a flow behaviour close to a plug-flow reactor in a closed vessel, the screw reactor is a good candidate for handling complex and exothermic (or endothermic) reactions [7–9]. For instance, screw reactors can be used for biomass pyrolysis [10], biomass hydrolysis [11], solid drying [6,12], etc.

The flow behaviour in such device is quite complex to predict, leading to some difficulties when designing screw conveyors. Many authors solved force and energy balances on solid particles in a screw conveyor. Therefore, theoretical equations are found to estimate the torque requirement [13–16] or the volumetric efficiency [15–17]. These analytical equations take into account the solid properties, the screw geometry and are generally in agreement with some experimental data. Yet, the assumptions made restrict the domain of application, and some cannot be applied, even for simple geometries [18,19].

Thus, the screw conveyor designing is usually developed from empirical results [20], leading to functioning issues [21]. Some guidelines can be found in the literature, such as the pitch length equal to the screw diameter and the shaft diameter equal to 35% of the screw diameter [3,5,22]. Rademacher [17] developed a model to size the gap screw/wall [23], which must be at least 1.5 times particle diameter higher. The filling degree, defined as the actual powder volume on the total volume in a pitch ratio [3,24], should not exceed 15% or 50%, depending on the solid abrasiveness [3,6,25]. Moreover, the volumetric efficiency, defined as the actual volumetric flow rate on the theoretical volumetric flow rate, decrease when increasing the rotation speed, the inclination angle of the screw conveyor [17,26] and the pitch length [15,19].

Finally, Waje *et al.* also proposed empirical graphics to evaluate the screw capacity with rotation speed, screw diameter and filling degree plus a stepwise procedure for a screw conveyor dryer [5]. Rademacher [22], with dimensional analysis, developed a model that predicts the screw conveying ability, depending on screw geometry. Rehkugler and Boyd [27] as well as Roberts and Wills [26] also developed a dimensionless model to predict the torque and power requirement or screw conveying capacity, with geometric, operating and solid properties.

Even if the flow behaviour of a screw reactor is close to a plug-flow reactor, the hydrodynamic strongly depends on the filling degree. Indeed, Waje *et al.* described three different flow behaviour, depending on this parameter [2,4]. For a poor filling degree, the solid is well mixed in the pitch, giving a good local mixing, but the solid does not mix with other pitches. For moderate filling degree, around 20%, the solid is still well mixed in the pitch and passes over the screw shaft, flowing back to the previous pitch, increasing the global mixing. For a high filling degree, the screw is saturated, thus the local, at the scale of a pitch, and global, at the scale of the screw, mixing are highly reduced. In a screw conveyor, it generally operates between a poor and a moderate filling degree. Between these two types of flow, the hydrodynamic is different and must be studied separately.

Many authors studied the screw reactor hydrodynamic using Residence Time Distribution (RTD) experimentally [2,4,11,24,28]. Nachenius *et al.* [24], Sievers *et al.* [28] and Sievers and Stickel [11] proposed a linear model in order to determine the mean residence time according to the solid flow rate, the rotation speed or the screw geometry. These models can be useful when designing a screw conveyor.

Although hydrodynamics in a screw reactor has been widely studied, few articles discuss about powder flow behaviour in such reactor. Indeed, particles with diameter higher than 300 µm was mainly studied in the literature. Moreover, the models found in the literature are not enough developed to predict the hydrodynamic in a screw reactor, based on the powder properties (*i.e.* Hausner ratio), the screw geometry, etc. In this work, we studied the RTD in a screw reactor involving powder, with different geometries and different material properties. We also compared two different methods of powder hydrodynamics characterisation and we used the Vashy-Buckingham theorem to build a dimensionless model that is able to predict the RTD in a screw reactor. The dimensionless model developed predicts with good accuracy our experimental results, as well as literature experimental data.

2. EXPERIMENTAL

2.1. Experimental device

Figure 1 shows a scheme of the experimental system. A feed conveyor (Brabender Screw Feeder DSR28) equipped with a hopper, feeds the screw conveyor studied. Mixing knives and the feed conveyor are both controlled by the same motor. Their rotation speeds are regulated with a set point (Linn, High Therm), varying from 0 to 140 RPM (±0.3 RPM). A computer controls the rotation speed of the studied screw conveyor from 0 to 7.5 RPM (±0.1 RPM). The outlet is connected to an exit bond, allowing to take samples in a flask. A scale can be placed below, to follow the mass over time during an experiment.

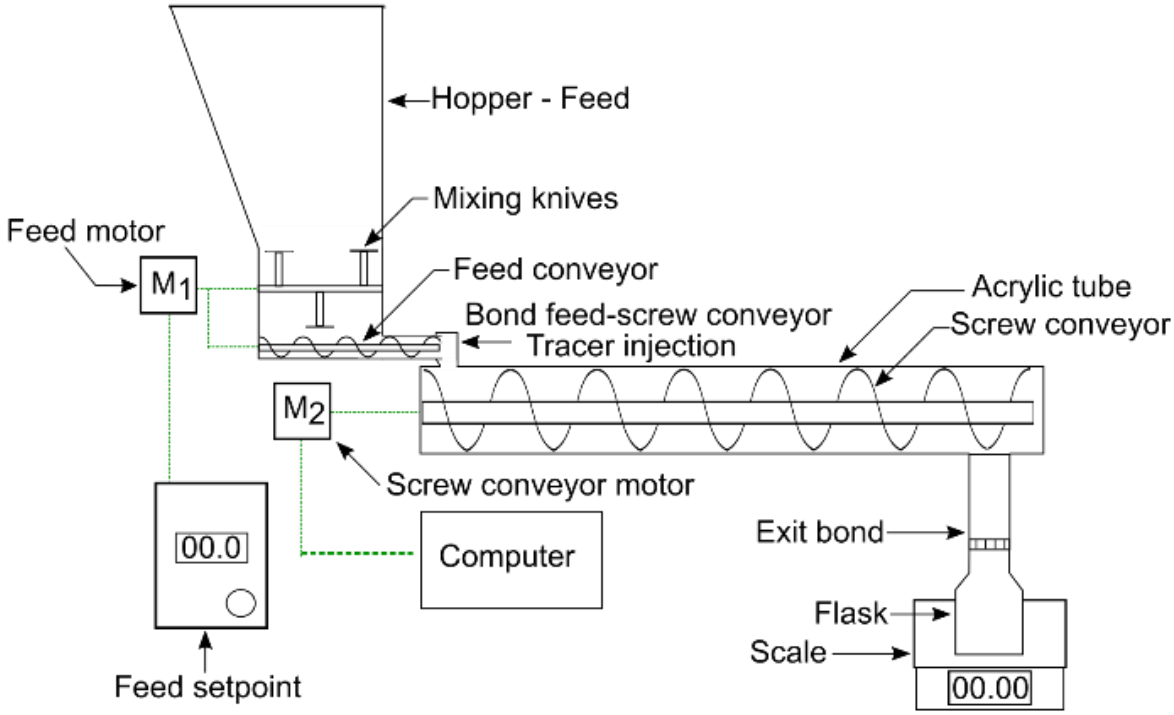

Figure 1: Scheme of the experimental system used for RTD measurement in a screw conveyor

Three screw conveyor geometries with their associated acrylic tube were studied. The acrylic tube allows to visualise the powder flow. Table 1 lists the characteristic dimensions of each screw reactor. The screws 1 and 2 are homothetic, with a 1.5 ratio. The screw 3 has the same dimension of screw 2, with a larger pitch. A steel tube was also available, in order to study the wall material effect, having the same dimension as the acrylic tube for the screw 2. Having this combination allows studying the geometry influence on RTD, precisely the pitch, the length and the screw diameter but also the reactor wall material with the steel tube.

Table 1: Dimensions of the different screw conveyors studied

Geometry	Screw 1	Screw 2	Screw 3
Screw Diameter D_{sc} (mm)	116	76	74
Shaft diameter D_{sh} (mm)	42	27	23
Inlet-Outlet Length L_{sc} (mm)	1471	964	841
Pitch length p_{sc} (mm)	35	23	35
Screw thickness e (mm)	5	3,5	3,7
Internal diameter of the tube D_{in} (mm)	120	80	80
Radial clearance (mm)	2	2	3

All the hydrodynamics studies were performed once a steady state was achieved. The steady state is assumed to be reached once the flow rate at the screw conveyor outlet is constant.

2.2. Powder used and their flowability properties.

In order to show the influence of powder material, three different powders were studied. Brown corundum F180 (Al_2O_3), defined by the standard FEPA 42 F 1984, glass powder (SR.PV GGR 160 40-80 µm) and rice flour (Molino Brunnati, Italia) were studied. All their flowability properties are listed in Table 2.

Many physico-chemical properties can be measured to determine the powder flowability. Regarding the functioning of a screw conveyor, the powder is continuously pushed and sheared with repeated avalanching [29]. Therefore, the static angle of repose and the Hausner ratio were considered to represent well the powder behaviour in such condition.

The static angle of repose, corresponding to the angle between the horizontal plane and the slope line of a powder heap, was measured with a funnel method (EFT 01 Electrolab©), which is adapted to the process [30]. The bulk and tapped density were measured, according to the standard NF ISO 9161. The Hausner ratio is the ratio of the tapped density over the bulk density. The Hausner ratio is used to assess the ability of a particle population to flow: the higher it is, the less flowable the powder is. The granulometric size distribution measurement (Mastersizer 3000E, Malvern) was performed in water for brown corundum and glass powder, and in ethanol for rice flour. All analyses were done under ambient temperature, pressure and moisture and were repeated at least 3 times.

Table 2: Flowability properties of studied powder

	ρ_{bulk} $(kg\ m^{-3})$	θ (°)	HR (-)	D_{10} (µm)	D_{50} (µm)	D_{90} (µm)
Brown corundum F180	1815	31	1.17	50	81	125
Glass powder	924	38	1.27	53	114	191
Rice flour	549	43	1.42	24	96	165

The D_{90} to the screw/tube gap ratio is less than 10%. It can be noticed that a small trend appears between these flowability properties: when the static angle of repose increases, the Hausner ratio increase. A poorer flowability means more cohesion force between solid particles, inducing a higher static angle of repose and Hausner ratio.

Beakawi Al-Hashemi and Baghabra Al-Amoudi reviewed the methods to measure the angle of repose [30]. Depending on the chosen methods and on the operator, the static angle of repose for the same powder can vary significantly. In our case, the maximum relative standard variation (RSD) was 5%.

Regarding the Hausner ratio, the main problem arises from the measurement of the bulk solid density. Indeed, it can be difficult to determine this density without tapping the solid. The method used here gives a low drop altitude to minimise the solid compression. The tapped solid density does not give such problem. In our case, the maximum RSD for the Hausner ratio was 4%. Therefore, in our case, the Hausner ratio is a more precise measurement of powder flowability compared to the angle of repose.

2.3. Determination of the overflow point

The filling degree, noted FD was calculated according to Waje *et al.* [6] from equation 1.

$$FD = \frac{(Qm/\rho_{bulk})}{N.\frac{\pi}{4}.(D_{in}^2 - D_{sh}^2).(p_{sc} - e)} \quad 1$$

When FD is high enough, the powder passes over the shaft, falling in the previous pitch, giving a different hydrodynamic pattern compared to a powder flowing down the shaft (Figure 2A). Such limit can be described as an overflow point, meaning that the powder passes over the shaft for a certain FD_{OF} value. Here, the overflow point is the limit powder volume that overflows over the shaft divided by the total pitch volume.

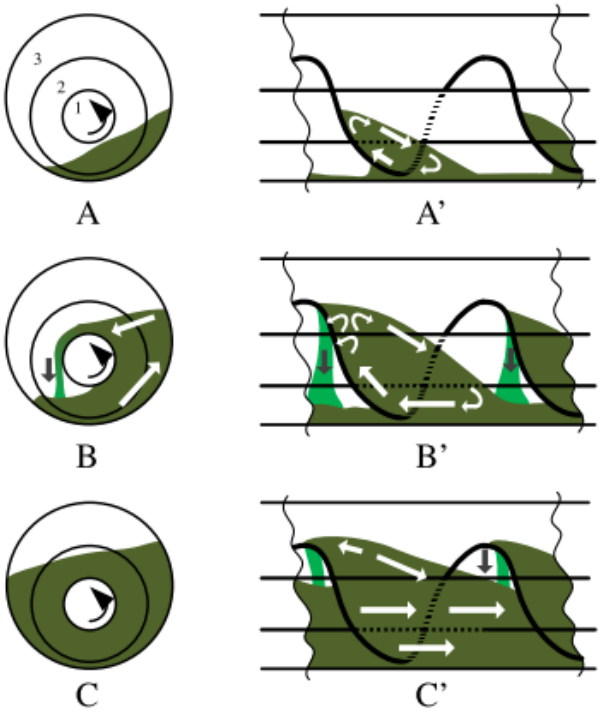

Figure 2: Flow pattern for different filling degree in a screw reactor [2,24]

The heap shapes are similar in each pitch with powder having good flowability (Figure 3a). However, with a powder having poor flowability, it can be different from a pitch to another (Figure 3b): the powder can overflow in a single pitch but not in every pitch. Thus, to determine this overflow point, for a given screw geometry and rotation speed, the inlet flow rate was adjusted until one or more particle started to flow over the shaft in every pitch at steady flow rate.

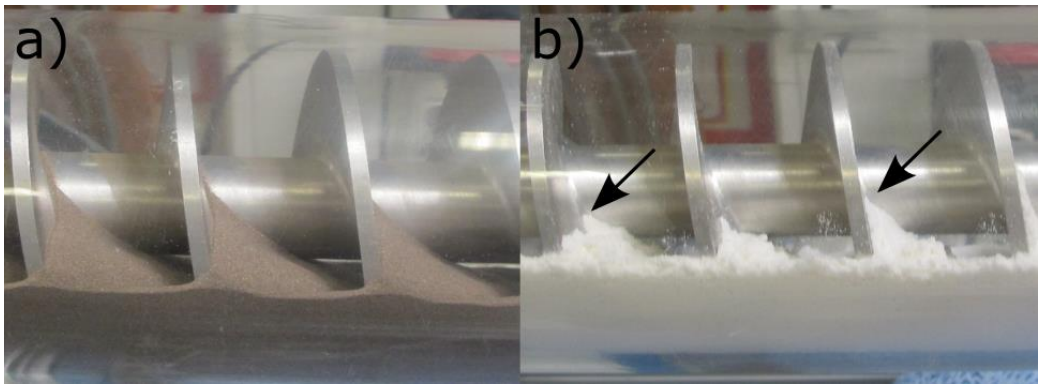

Figure 3 : heap shape in a screw conveyor with a) brown corundum F180 and b) rice flour.

2.4. Measure of residence time distribution

The RTD is a strong tool to understand the flow in a reactor. It gives relevant results about the flow pattern, such as the mean residence time or the axial dispersion. A tracer is injected at a precise location (generally at the inlet), either continuously (step) or instantaneously (pulse), and its concentration is monitored at the reactor outlet [31]. For solid materials, many types of tracer exist [2]. It is important to select a tracer with properties similar to its environment, especially with similar granulometry distribution and density [31–33]. Indeed, the tracer must: have properties similar to the powder studied, be non-interactive with the studied system, not adherent with the reactor wall and be detectable [31,32]. Generally, the tracer choice is a compromise between the tracer and the measurement system price, the precision and the ease of the measurement [32].

The RTD in powder flow is quite complex to measure, as a small perturbation must be done in order to visualise how the system reacts, without changing the overall hydrodynamic. For instance, Nachenius *et al.* results shows high variation of RTD results from flow rate variation study [24]. Chamberlin *et al.* compared two RTD measurement methods, one with flow rate variation and one with salt injection, which gave different results, up to 50% variation [34]. They discovered that the negative step flow rate variation gave larger RTD, possibly because some materials remained in the screw or the backflow is reduced during this RTD measurement. The reason for these RTD differences is not fully understood and must be investigated.

Two methods were compared to characterise the powder hydrodynamics. The first one, which studies the transitional state, consists of imposing a constant feed rate variation (step) [4,6,24]. The feed rate variation is done when the powder flow is stationary (*i.e.* constant flow rate at the exit). The feed rate at the reactor inlet is quickly increased (positive step) or decreased (negative step) and the mass variation at the reactor outlet is followed over time with a scale (Sartorius, $\pm$0.01g). The mass and time are noted at each revolution time when the screw flight passes over the screw outlet. The mass flow rate can be calculated over time, giving the response to the feed rate variation at the inlet. The measurement is stopped once the exit flow rate becomes stable again.

The second method, which measures the RTD, involves the rapid injection of a small amount of salty powder (pulse) at the reactor inlet (Figure 1). This injection is done when the flow is stationary. The salty powder is prepared by well-mixing the studied powder with a highly saturated saline solution (approximately 340 g/L with salt, Anhydrous Redi-Dri™, Sigma Aldrich). The solution is then filtered, the cake from the suspension is dried in an oven at 150 °C and the powder is sieved to its initial granulometric size distribution (less than 125 µm). This method is not adapted for rice flour as rice flour interacts with water. Therefore, a blend of rice and salt, used for the saline solution and sieved at less than 125 µm, with some rice flour was prepared and injected in the screw reactor. Once the pulse is done at the inlet of the screw (Figure 1), a sample is collected at the reactor outlet at each revolution time, when the screw flight passes over the screw outlet. The time between the pulse and the sample collection is noted. The sampling is performed until the measurement duration reaches 1.5 the time of passage. After collecting all the samples from the RTD, each of them was poured in a beaker containing distilled water and the suspension was thoroughly mixed. After decantation, the solution was analysed with a conductimetric probe (Lab 970, SI Analytics, $\pm 10\ \mu S$/cm), initially calibrated for saline solution from 0 to 100 g/L. Knowing the sample collection time and its concentration, the tracer concentration over time can be measured.

2.5. Data processing

2.5.1. Data analysis

In order to study the powder hydrodynamics in transitional state, a flow rate variation curve, noted F_v, is calculated with equation 2. The F_v curve represents the variation of the mass flow rate at the outlet after a flow rate variation at the inlet, giving the transitional state evolution towards a stationary state.

$$F_v(t) \approx \frac{Q_{m,initial} - Q_m(t_i)}{Q_{m,initial} - Q_{m,final}} \quad (2)$$

$Q_{m,initial}$ and $Q_{m,final}$ are respectively the initial and final powder mass flow rate at the reactor outlet during the flow rate variation measurement, $Q_m(t_i)$ is the powder mass flow rate at the reactor outlet measured at each revolution time. For the RTD measurement, depending on the tracer injection, the response to a pulse can be described with the probability distribution function E(t) (equation 3) and the response to a step is treated with the cumulative distribution function F(t) (equation 4), which both can be determined from the other one.

$$E(t) = \frac{c_{I,pulse}(t)}{\int_0^\infty c_I(t)dt} \quad (3)$$

$$F(t) = \frac{c_{I,step}(t)}{c_0, step} = \int_0^t E(t').dt' \quad (4)$$

With $c_{I,pulse}(t)$ and $c_{I,step}(t)$ respectively the tracer concentration at the screw conveyor outlet over time for a pulse and step experiment and c_0 the constant inlet tracer concentration injected for a step experiment. For the salty powder injection, each sample was analysed over time, giving a discretisation of the E(t) function [35].

$$E(t) \approx \frac{c_{pulse}(t_i)}{\sum_{i=0}^{Ns} c_{pulse}(t_i)\Delta t_i} \quad (5)$$

Where $c_{pulse}(t_i)$ is the tracer concentration at the sampling time i, N_s is the total number of samples, Δt_i is the time difference between sample collections. The RTD analysis is generally done by calculating the first and the second-centred moments. The first one is noted $\bar{t}$ and gives the mean residence time, the second (centred) is noted σ^2 and gives the variance of the residence time distribution [31,35].

$$\bar{t} = \int_0^\infty t.E(t).dt \approx \sum_i^{N_s} t_i.E(t_i).\Delta t_i \quad (6)$$

$$\sigma^2 = \int_0^\infty (t-\bar{t})^2.E(t).dt \approx \sum_i^{N_s} (t_i-\bar{t})^2.E(t_i).\Delta t_i \quad (7)$$

2.5.2. Gamma distribution and compartment models

The variance of a E(t) curve calculated with equation 7 can be distorted by an asymmetry. To represent this asymmetry, a gamma distribution defined in equation can be used 8.

$$E(t) = \frac{1}{b^a.\Gamma(a)}.(t-t_0)^{a-1}.\exp\left(-\frac{t-t_0}{b}\right) \quad (8)$$

This function is similar to a Gaussian distribution, with an asymmetric term characterised by the skewness of the signal, noted s. The mean residence time and the variance are also related to the gamma distribution.

$$a = \frac{4}{s^2} \quad (9)$$

$$b = \frac{1}{2}.\sigma.s \quad (10)$$

$$t_0 = \bar{t} - 2.\frac{\sigma}{s} \quad (11)$$

Another way to represent the RTD curve is to find the association of ideal flow reactors, such as Continuous Stirred Tank Reactor (CSTR) or Plug-Flow Reactor (PFR), with dead zones, bypass flow, recycle flow, etc. that best described the RTD curve [35]. The parameters in such models are generally the volume of each ideal flow reactor, the flow proportion of recycling, etc. For example, a PFR in series with a CSTR leads to equation 12 [35,36], with Q the material flow rate, V_{CSTR} and V_{PFR} respectively the CSTR and PFR volume.

$$\begin{cases} E(t) = 0 & \forall t < \tau_{PFR} \\ E(t) = \frac{Q}{V_{CSTR}}.\exp\left(-\frac{Q}{V_{CSTR}}.t + \frac{V_{PFR}}{V_{CSTR}}\right) & \forall t \geq \tau_{PFR} \end{cases} \quad (12)$$

3. RESULTS AND DISCUSSION

3.1. Overflow point results and modelling

The overflow point measurement was studied for different screw geometries, rotation speeds and powder flowability (Figure 4). The Froude number, comparing the inertia force imposed by the screw on the powder over the gravitational force as $Fr = \frac{D_{SC}.N^2}{g}$, allows seeing the rotation speed influence on the overflow point for different screw geometry. In our case, the inertia forces are very low, explaining why a poor trend can be noticed here. Yet, it shows that increasing the rotation speed, thus the Froude number, seems to modestly decrease the overflow point. It can be expected that increasing the rotation speed would result in a lower FD_{OF} value, as the powder would follow the screw rotation and be lifted more.

Table 3: Experimental data for the overflow point

			Brown corundum F180	Glass powder	Rice flour
	Fr (-)	p_{sc}/D_{Sc}	FD_{OF} (%)	FD_{OF} (%)	FD_{OF} (%)
Screw 1	7.46×10^{-7}	0.30	32	31	32
Screw 2	2.97×10^{-7}	0.30	32	31	29
	1.97×10^{-6}	0.30	31	32	27
	7.88×10^{-6}	0.30	31	29	26
Screw 3	2.91×10^{-7}	0.47	26	19	19
	1.97×10^{-6}	0.47	24	20	19
	7.88×10^{-6}	0.47	24	20	18

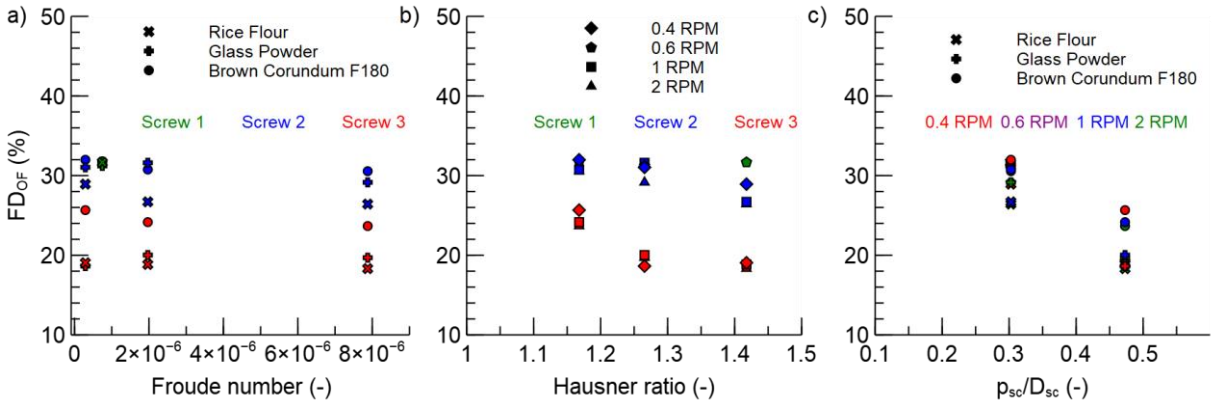

Figure 4: Overflow point variation with a) rotation speed, b) powder flowability and c) pitch length

Regarding the powder flowability, increasing the Hausner ratio reduces the overflow point. As the powder cohesiveness increases, the heap formed inside the screw pitch, related to the static angle of repose (Table 2), gains more altitude. Therefore, a powder with poor flowability overflows more easily.

The pitch to screw diameter ratio also affects the overflow point. A lower pitch to screw diameter ratio gives a higher screw flight inclination angle, compared to the rotation axis. The powder is more easily lifted up, thus overflow with a lower filling degree. Moreover, a power with less flowability will more likely be pushed up by the blade, as the particles remain close to the screw flight.

A dimensionless model can be used to correlate the non-dimension number with the overflow point FD_{OF} (equation 13). The model was fitted with the experimental data from Table 3. The parameters and their standard deviation are listed in Table 4.

$$FD_{OF} = K.(Fr)^{a}.HR^{b}.\left(\frac{p_{SC}}{D_{SC}}\right)^{c} \quad 13$$

Table 4: Parameters and their standard deviation for the overflow point prediction (equation13)

Parameter	Value	Standard deviation
K	0.107	0.018
a	-0.018	0.011
b	-0.730	0.172
c	-0.804	0.068

The parity plot (Figure 5) shows that the model represents with good accuracy the experimental data. This model can predict whether the powder passes over the shaft or not, knowing its geometry, the Hausner ratio and the operating conditions. Predicting the overflow point helps to select the operating conditions regarding of the reaction or treatment process. Indeed, a solid flow below the shaft leads to a more compact flow, with little mixing between pitches, whereas a solid flow over the shaft creates a higher global mixing (Figure 2).

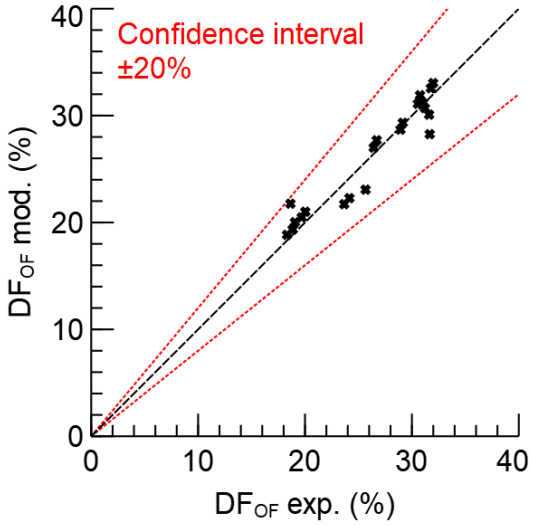

Figure 5: Parity plot comparing the experimental and predicted overflow point with equation 13 using parameters from Table 4

3.2. Flow rate variation study

Feed rate variation of 100% (quick start or stop) were studied with brown corundum F180 (screw 1), glass powder (screw 3) and rice flour (screw 3). The flow rate variation curves, calculated with equation 2, are plotted on Figure 6 and the results are shown in Table 5.

Table 5: Results from the flow rate variation study

Exp.	HR (-)	FD (%)	Fr (-)	$\frac{p_{SC}}{D_{SC}}$ (-)	Step	$\bar{t}/\tau$ (-)
A	1.17	9	4.71×10^{-6}	0.47	Positive	1,19
B					Negative	1,17
C	1.42	8	1.17×10^{-6}		Positive	1.01
D					Negative	1.05

In each case, the step function can be clearly seen. For powder with good flowability (*i.e.* brown corundum F180), the system takes less time to stabilise when started compared to negative variation. Indeed, the steady state in the positive variation appears at approximately $t = 1.2\tau$ (Figure 6a), while for the negative variation at approximately $t = 1.3\tau$ (Figure 6b), with $\tau = \frac{L_{SC}}{N.p}$ the conveyor time of passage [24,34]. Such results were also found by Chamberlin *et al.* [34]. Moreover, the steady state takes a longer time when the FD value is higher than FD_{OF}, especially for a quick stop. As the solid flows over the shaft, there are more flow fluctuations, increasing the time needed to reach the steady state.

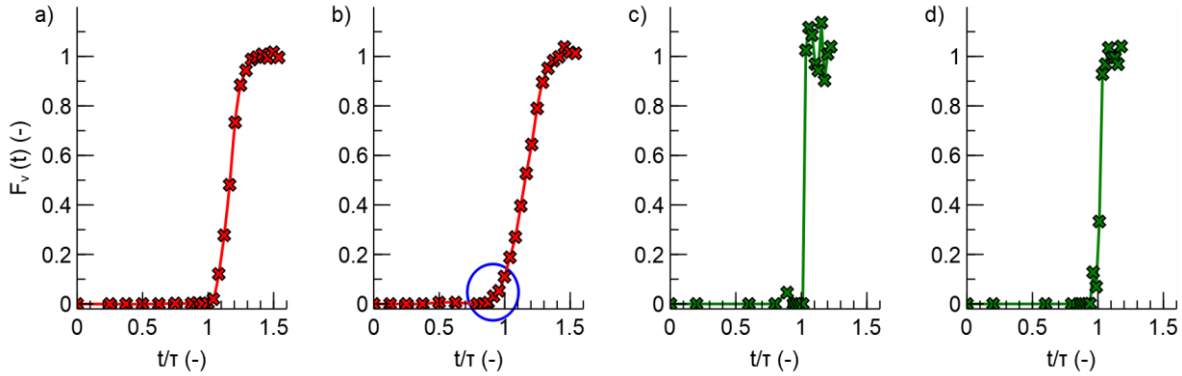

Figure 6: Flow rate variation with quick a) start and b) stop (brown corundum F180, FD=9%<FD_{OF}, Fr=4.71×10^{-6}, HR=1.17), c) start and d) stop (rice flour, FD=8%<FD_{OF}, Fr=1.17×10^{-6}, HR=1.42)

For a quick start, the flow rate appears exactly at the conveyor time of passage. It means that the solid in a pitch does not exchange with the next one, which is understandable as the powder mainly moves at the screw rotation speed [37,38]. Yet, for a quick stop, the flow rate decreases before the conveyor time of passage. Indeed, with brown corundum F180, the mass flow rate diminishes two revolution times before the conveyor time of passage (Figure 6b). However, for a poor flowability powder (*i.e.* rice flour), the quick start and stop are similar (Figure 6c and d) and synchronised with the time of passage.

To explain the hydrodynamic difference between a quick start and a quick stop, heap formed during the conveying flows forward, in the conveying direction. Yet, a small amount of powder is not directly pushed by the screw as it is located in the screw/tube gap. Therefore, this quantity of powder does not follow the screw progression and remains motionless. It flows in the pitch behind, resulting in a “backflow” (compared to the conveying direction).

This “backflow” is directly linked to the filling degree; if the filling degree is low, the backflow is more important as there is more free space for the powder to flow in the pitch behind. Inversely, if the pitch is more filled, the powder can no more flow backward, blocked by the powder heap in the pitch behind. The Figure 7a represents a quick start, the pitch is full, reducing the backflow in the screw/tube gap (red arrow). For a quick stop (Figure 7b), the pitches are getting emptied, increasing the backflow. Thus, the flow in the conveying direction is reduced, explaining its reduction before the conveyor time of passage, in a case of a quick stop.

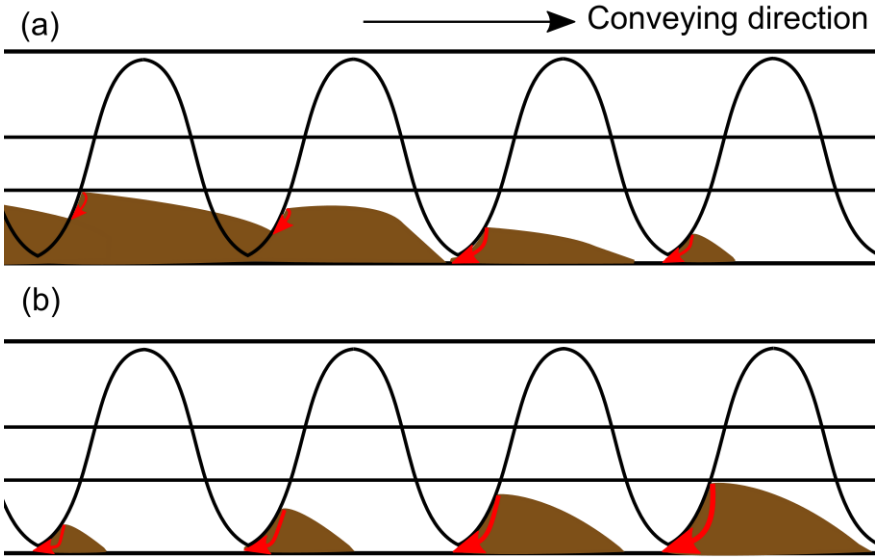

Figure 7: Representation of a flow rate variation for a) quick start and b) quick stop

The flow rate variation measurement is not convenient in this case. Indeed, the backflow in the screw/tube gap is affected by the filling degree. Nachenius *et al.* also found that varying the flow rate or the rotation speed, which is directly linked to the filling degree, affects the hydrodynamic, disturbing the results obtained from it (high variation) [24].

Even if these flow rate variation curves are not representative of the steady state reactor hydrodynamic, some information can be taken from it. First, the system responds quickly to a perturbation: the flow rate stabilises rapidly when the flow rate is changed, around 30% more than the conveyor time of passage. Powder with poor flowability (high Hausner ratio) will lead to a quicker steady state, compared with good flowability powder. Moreover, the powder contained in one pitch does not communicate with the next one. Thus, the powder leaves out the screw conveyor at the conveyor time of passage, which can be interpreted as a delay demonstrating the plug-flow behaviour. Finally, the filling degree affects the hydrodynamic in such reactor, as seen in a quick stop flow rate.

3.3. Validation of the RTD measurement with salty powder injection

Before running the RTD measurement experiments, the tracer properties were analysed and compared with the original powder. Regarding the granulometric size distribution analysis, it was performed in water for the original powder, while for the salty ones and for the rice flour, it was analysed in ethanol. The bulk density and the static angle of repose of salty powders were also measured. Table 6 summarises the results obtained. Compared with Table 2, the tracer and original powder have similar properties. Moreover, only a small amount of this tracer was injected for the RTD measurement, up to 5% of the total mass pitch. It means that such tracer should not disturb the overall solid flow in the screw conveyor.

Table 6: Flowability properties of salty powder used as tracer

	ρ_{bulk} $(kg\ m^{-3})$	θ (°)	D_{10} (µm)	D_{50} (µm)	D_{90} (µm)
Salty Brown corundum F180	1838	32	48	76	113
Salty glass powder	906	36	50	109	175

From the overflow point and the flow rate variation study, it has been concluded that the filling degree modifies the hydrodynamic and two different flow patterns exit: one with the powder flowing below the shaft ($FD<FD_{OF}$) and one with the powder flowing over the shaft ($FD>FD_{OF}$). Therefore, the repeatability of the RTD measurement was verified for $FD<FD_{OF}$ and for $FD>FD_{OF}$. For $FD<FD_{OF}$ (Figure 8a), three experiments with the same amount of tracer (5% of pitch mass) were done, two others with changing the amount of tracer injection (7.5% and 10% of pitch mass) and another one with a blend of brown corundum F180 and 125 µm sieved salt (5% of pitch mass). For $FD> FD_{OF}$ (Figure 8b), two experiments with the same amount of tracer (5% of pitch mass) were also repeated. Details on the error bars calculation is given in the appendix.

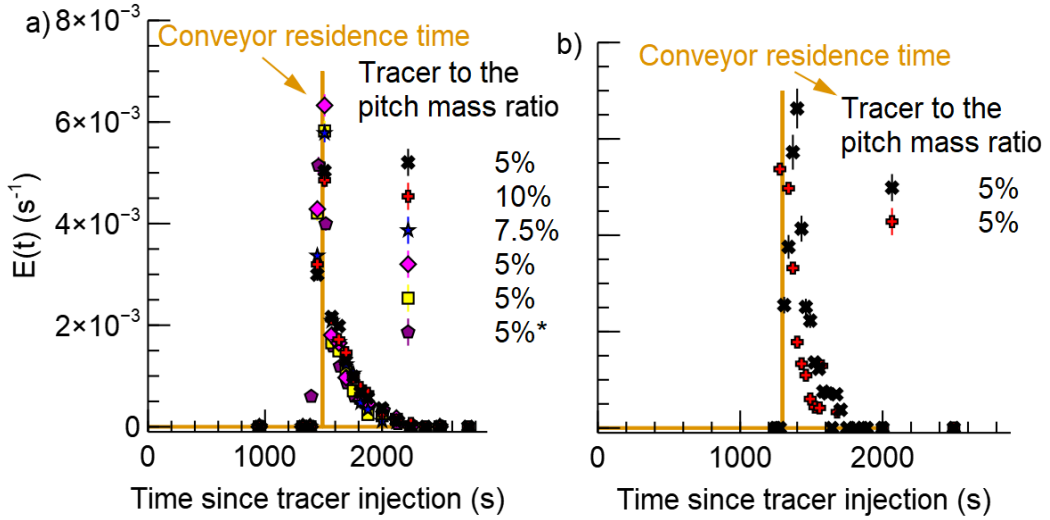

Figure 8: Study of the tracer mass to the pitch mass ratio in a pitch ratio injected and verifying the repeatability with brown corundum F180 and with screw 3 (*with sieved salt) a) for FD=20%<FD_{OF} and Fr=1.96×10^{-6} and b) for FD=40%>FD_{OF} and Fr=8.09×10^{-6}

With a FD<FD_{OF} the repeatability is verified, as the curves are overlapped (Figure 8a). It means the tracer injection with salty powder and with sieved salt below 125 µm is adapted. It also means that the sieved salt with rice flour should also be convenient. Even if an amount of tracer equal to 10% of pitch mass does not change the RTD, the next measurements were always performed with 5% of pitch mass, as the signal is visible enough. Yet, for FD> FD_{OF}, the curve are slightly different (Figure 8b). For a high FD, the powder in the pitch before the one passing over the exit starts to flow down the sample (Figure 9), creating a bypass. For a high filling degree, the powder mixing seems to be reduced due to the lack of space inside a pitch. The tracer concentration can be less homogeneous inside the powder heap compared to low filling degree. Moreover, phenomena at high filling degree are different from low filling degree, such as overflow and bypass. All these reasons can affect the repeatability. Yet, the curves are only shifted by one time of revolution, which is negligible regarding of the conveyor time of passage (less than 4.2%).

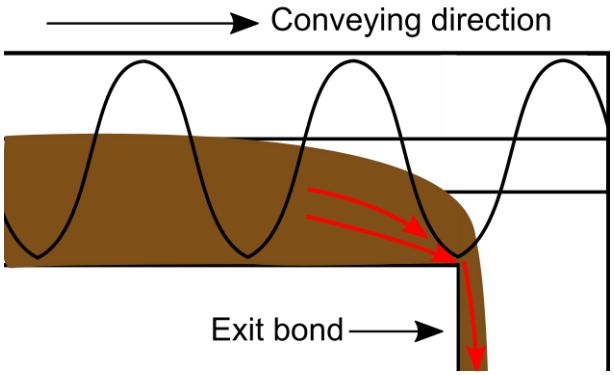

Figure 9: Bypass at the exit bond for high filling degree

The RTD curves (Figure 8), have a particular shape: a peak appears when the time since tracer injection is equal to the conveyor time of passage, then the curve decreases exponentially. For screw reactors, such shape can be found in the literature [2,11,28]. As the powder is continuously pushed by the screw, most of the powder flows out of the reactor at the time of passage, explaining the peak. Moreover, the tracer dispersion either take place in the screw tube gap (FD<FD_{OF}) or with the overflow (FD>FD_{OF}). In both cases, the powder amount dispersed in the reactor is lower than the powder amount pushed by the screw, causing this exponential decay.

The results are summarised in Table 7. The standard deviation was calculated from all the repeatability experiment according to the sample standard deviation equation. It can be seen that the relative standard deviation is low for the mean residence time, but it is rather high for the variance, although the curves are overlapping. Such deviation on σ^2 can also be found in the literature [39]. As σ^2 depends on $\bar{t}^2$ and on $E(t)$ (equation 7), its deviation is at least higher than four times the deviation from $\bar{t}$.

Table 7: Repeatability results for RTD measurement

FD (%)	Fr (-)	% tracer mass	$\frac{\bar{t}}{\tau}$ $(-)$	$\frac{\sigma^2}{\tau^2}$ $(-)$
20	1.97×10^{-6}	5	1.08 ± 0.02	$(1.19 \pm 0.19).10^{-2}$
		10	1.09 ± 0.02	$(1.43 \pm 0.23).10^{-2}$
		7	1.07 ± 0.02	$(9.07 \pm 1.43).10^{-3}$
		5	1.04 ± 0.02	$(6.45 \pm 1.02).10^{-3}$
		5	1.04 ± 0.02	$(1.18 \pm 0.19).10^{-2}$
		5	1.07 ± 0.02	$(1.25 \pm 0.20).10^{-2}$
40	8.09×10^{-6}	5	1.10 ± 0.04	$(4.51 \pm 0.86).10^{-3}$
		5	1.06 ± 0.04	$(5.98 \pm 1.14).10^{-3}$

3.4. Comparison of RTD model

As said in the experimental section, there are two common models to represent a RTD curve: the gamma distribution and the compartment model. Here, we compared these two models and found the one that best represents the RTD shape and is the most suitable.

3.4.1. Gamma distribution

Figure 8 shows that the E(t) function diverts from a plug-flow reactor, with a large signal spread, giving an asymmetric curve. Sievers *et al.* also found such behaviour [11,28] and they treated the signal with a gamma distribution, defined in equation 8.

Therefore, the mean residence time, the variance and the skewness were calculated with the gamma distribution by using the least squares method between this model and the experiment values. The mean residence time and the variance were initialised from equations 6 and 7.

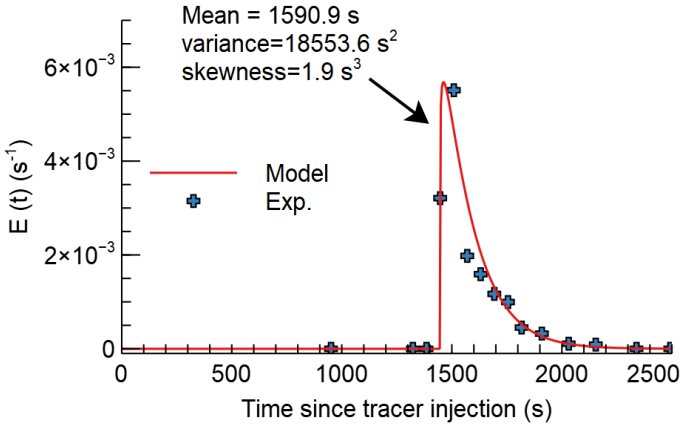

Figure 10: Gamma distribution fitted for FD=20%<FD_{OF} and Fr=1.96×10^{-6}

Figure 10 shows the gamma distribution fitted to one of the repeated experiments from Figure 8. It can be seen that this model represents accurately the RTD in a screw conveyor. Yet, this model needs three parameters to fit the experimental data. Moreover, fitting a modified probability distribution on an asymmetry distribution may not be that appropriate [35].

3.4.2. Compartment model

The RTD shape (Figure 8) shows a delay, followed by a quick emergence and an exponential decrease. The layout model of a PFR followed by a CSTR in series is the most representative [35]. We defined some terms before fitting the compartment model (equation 14).

$$\begin{cases} V_{reac} = Q.\tau \\ V_{RTD} = Q.\bar{t} \\ V_{RTD} = V_{PFR} + V_{CSTR} \end{cases} \quad 14$$

With V_{reac} the reactor volume, V_{RTD} the RTD volume, V_{PFR} and V_{CSTR} respectively the PFR and CSTR volume. The RTD function can be calculated with the equation 12 [35]. Here, we defined $\tau_{PFR} = \frac{V_{PFR}}{Q}$. For a practical reason, we introduced the PFR and CSTR volume proportion ($p_{PFR} = V_{PFR}/V_{reac}$ and $p_{CSTR} = V_{CSTR}/V_{reac}$). It means that $p_{PFR} + p_{CSTR} = \frac{\bar{t}}{\tau}$. Hence, equation 12 can be arranged in equation 15.

$$\begin{cases} E(t) = 0 & \forall t < \tau_{PFR} \\ E(t) = \frac{1}{\tau.p_{CSTR}}.\exp\left(-\frac{t-\bar{t}+\tau.p_{CSTR}}{\tau.p_{CSTR}}\right) & \forall t \geq \tau_{PFR} \end{cases} \quad 15$$

Finally, knowing τ and using $\bar{t}$ from the RTD results, this compartment model can be fit on the experimental data by adjusting p_{CSTR} (or p_{PFR}) and minimising the least square between the experimental data and the model data.

The model represents accurately the RTD results, especially the exponential decrease (Figure 11). It means that the powder moves at the screw speed, with some mixing in between the pitches (backflow). The sum of PFR and CSTR volume proportion is slightly higher than 1, which means that the mean residence time is close but greater than the conveyor time of passage. This result is in agreement with the literature [24,34,40] and may reflect a dynamic powder retention during operation.

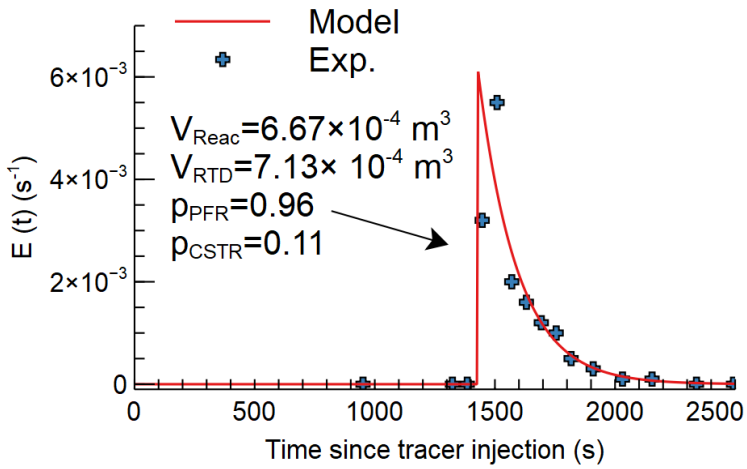

Figure 11: Compartment model for a PFR with a CSTR in series for FD=20%<FD_{OF} and Fr=1.96×10^{-6}

It can be seen that the p_{PFR} is much greater than the p_{CSTR}, showing again the plug flow behaviour of the screw reactor. The global mixing is characterised by p_{CSTR}, which is low but not negligible.

3.5. Scanning the operating parameters that influence the RTD

A prospection on the operating parameters that may change the RTD was done in the experimental domain, using the screw 3. This involves the variation of the filling degree, the Froude number and the Hausner ratio. In order to compare the results, the time since tracer injection and the E(t) function are respectively divided and multiplied by the conveyor time of passage τ. It is usually divided by the mean residence time [4,39], but this way is more convenient to visualise any difference.

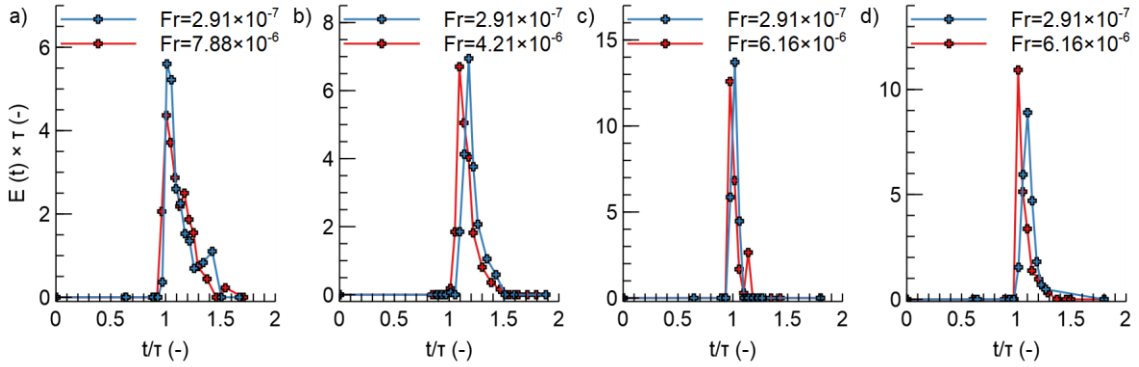

Figure 12: Influence of the filling degree (FD), the Froude number (Fr) and the powder properties (Hausner ratio) on the residence time distribution with screw 3: a) FD=10%, HR=1.17 (brown corundum F180), b) FD=40%, HR=1.17 (brown corundum F180), c) FD=10%, HR=1.42 (rice flour) and d) FD=40%, HR=1.42 (rice flour)

First, it appears that, in these conditions, the Froude number does not have a significant impact on the RTD shape (Figure 12) nor on the RTD results (Table 8). Indeed, when multiplying the Froude number by approximately 27, at FD=10%, the RTD curves overlap (Figure 12a and c, Table 8 Exp. A,B and E,F), while for FD=40%, there is a small deviation (Figure 12b and d, Table 8 Exp. C,D and G,H). Such deviation for FD=40% is in agreement with the repeated experiment (Figure 8b). For small rotation speed, the powder has time to be at its repose state. Increasing the Froude number only changes the conveyor time of passage, but not the mixing efficiency. Such conclusion has been observed in a rotary kiln [41].

Table 8: Results from the scanning of the experimental domain

Exp.	HR (-)	FD (%)	Fr (-)	$\frac{p_{SC}}{D_{SC}}$ (-)	$\frac{\bar{t}}{\tau}$ (−)	p_{CSTR} (-)
A	1.17	10	2.91×10^{-7}	0.47	1.16	0.17
B			7.88×10^{-6}		1.13	0.17
C		41	2.91×10^{-7}		1.20	0.08
D			4.21×10^{-6}		1.16	0.11
E	1.42	10	2.91×10^{-7}		1.01	0.03
F			6.16×10^{-6}		1.02	0.05
G		37	2.91×10^{-7}		1.08	0.07
H			6.16×10^{-6}		1.07	0.07

The Table 8 shows that the RTD depends significantly on the powder flowability. For a powder with good flowability, such as the brown corundum F180 with HR=1.17, it can flow in between the screw/tube gap, increasing the curve spread (high p_{CSTR}). For rice flour, the powder was almost unable to flow in between this gap, suppressing the global mixing. It can be seen when comparing Figure 12a and c as well as Table 8 Exp. A, E or B,F.

Moreover, the filling degree does modify the hydrodynamic, validating the observations from the flow rate variation study. For FD=40%, the mean residence time to conveyor time of passage ratio is greater than for FD=10% (Table 8 Exp. A,C or E,G). When FD=10%, the powder does not flow over the shaft (Figure 13a). In this case, for a powder with good flowability (*i.e.* brown corundum F180), a small amount of powder flows in the pitch behind through the screw/tube gap (Figure 13a'). For a powder with poor flowability (*i.e.* rice flour), the powder is not able to flow through the screw/tube gap, giving a $\bar{t}/\tau$ close to 1 (Table 8 Exp. E and F). When FD=40%, the flow is modified: the powder cannot flow in the screw/tube gap anymore or very hardly (Figure 13b'), but it flows over the shaft (Figure 13b). In this case, a larger powder amount flows in the pitch behind.

Eventually, with FD=10%, a powder with poor flowability is unable to flow in the pitch behind, but it can for FD=40% (Figure 13b), giving a larger p_{CSTR} (Table 8 Exp. E,G or F,H). In the case of a powder with good flowability, it is the opposite: the p_{CSTR} value is higher at FD=10% (Table 8 Exp. A,C or B,D). As there is less powder for FD=10%, the powder is free to flow in the pitch behind through the screw/tube gap (Figure 13a'). Once the powder flows in the pitch behind, it stays close to the screw/tube gap, where it can disperse easily along the screw. In the case of FD=40%, once the powder has overflowed in the pitch behind (Figure 13b'), it has to flow from the bottom to the top of the heap to overflow again (Figure 13b). Therefore, the path taken by the powder is longer, reducing its dispersion.

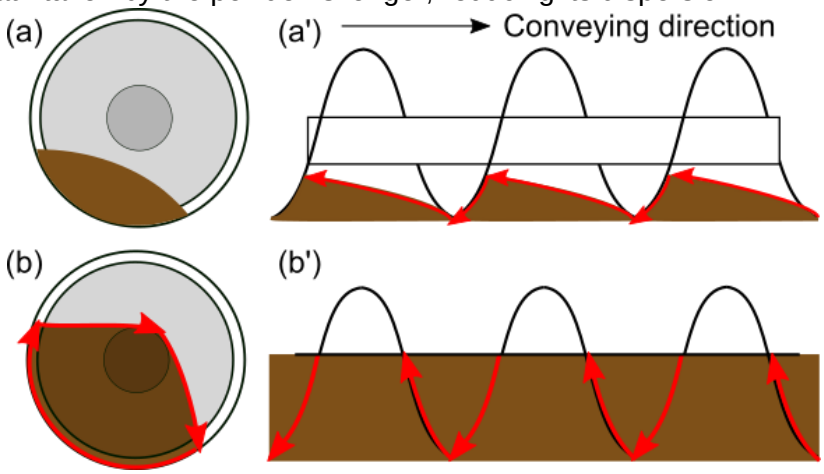

Figure 13: Powder dispersion represented with red arrows for different filling degree with good flowability: (a) cross section and (a') front view for low filling degree, (b) cross section and (b') front view for high filling degree.

This scanning shows that mainly the powder flowability (Hausner ratio) and the filling degree affect the RTD shape. In our condition, the Froude number does not have significant effect on the RTD. The literature shows that varying the rotation speed at constant flow rate changes the RTD : increasing the rotation speed enhances the RTD spread, thus the global mixing [2,11]. When the powder flows below the shaft and for a constant flow rate, increasing the rotation speed diminishes the filling degree, improving the backflow in the screw/tube gap. Meise *et al.* show that the dimensionless RTD at different rotation speeds are similar, if the filling degree is kept constant [42]. Such information is in agreement with our results.

3.6. Geometric and reactor wall material influence study on the RTD

Three different screws were used for the RTD measurement, to evaluate the geometry and the wall material influence (Table 1). The Figure 14 shows the results obtained for the geometric influence with brown corundum and for the wall material influence with rice flour.

It can be seen that the pitch length has a significant effect on the RTD (Figure 14a). Reducing the pitch narrows the RTD curve, inducing that the global mixing is lower (smaller p_{CSTR}). For a shorter pitch, there is more screw flight in the screw conveyor. The forward movement of the screw is enhanced, limiting the tracer exchange between pitches.

Regarding the screw length, the RTD curves are almost overlapping (Figure 14b). It means that for a 15% length variation, the global mixing is unchanged. This is in agreement with the previous results found. The flow behaviour is close to a plug flow reactor and the regime becomes quickly stationary. Thus, increasing the conveyor time of passage, directly linked to the screw length, has no significant effect on the RTD shape with a 15% length variation.

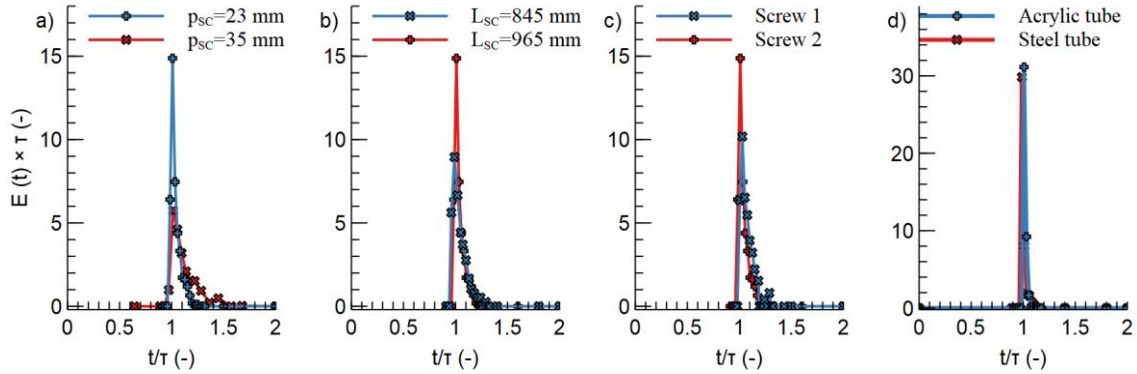

Figure 14: Geometry and wall material influence on the residence time distribution with a), b) and c) brown corundum F180 at FD=10% and d) rice flour at FD=40%

The scale up change influence was also studied on the RTD, comparing screws 1 and 2 (Table 1). All the screw 1 geometric dimensions were divided by a factor of 1.5. For such a change, the RTD curves are rather close (Figure 14c). It means that a dimensionless model developed in this study can be used for scaling up a screw reactor (see next section).

As the RTD measurements with salty powder pulse were run in an acrylic cylinder, it is important to know if the reactor wall material has any effect on the global hydrodynamic. A steel tube, having the same geometric dimensions of the acrylic tube for screw 2, was studied. As the RTD measurements are repeatable (Figure 8), three RTD were measured with this steel tube at 1 RPM: two with rice flour with different filling degree (FD=10% and FD=40%) and one with glass powder at FD=10%. The RTD with rice flour at FD=40% is plotted on Figure 14d. It can be seen that the RTD are similar when it is measured in an acrylic or steel cylinder. Therefore, all the RTD measurements and analyses obtained from acrylic tube can be extended to a steel wall reactor.

3.7. Parametric study of the dimensionless model

The compartment model seems to be more suitable, as it only needs two parameters, either p_{CSTR}, or p_{PFR}, and the mean residence time compared to the gamma distribution that needs three. Moreover, the screw length and the pitch length are correlated between screw 2 and screw 3: the pitch length is increased, but the screw length is reduced (Table 1). Therefore, only one geometric parameter must be chosen. From Figure 14, it has been concluded that the pitch length has greater effect on the RTD results than the screw length. Yet, a dimensionless model will be used to correlate the non-dimension number with the mean

residence time to the conveyor residence time ratio (equation 16 and with the p_{CSTR} proportion (equation 17), as p_{CSTR} represents the global mixing.

$$\bar{t} = \left(\frac{L_{SC}}{N.p}\right).k.(FD)^{\alpha}.(Fr)^{\beta}.HR^{\gamma}.\left(\frac{p_{SC}}{D_{SC}}\right)^{\delta} \quad (16)$$

$$p_{CSTR} = k'.(FD)^{\alpha'}.(Fr)^{\beta'}.HR^{\gamma'}.\left(\frac{p_{SC}}{D_{SC}}\right)^{\delta'} \quad (17)$$

From section 2.2, it has been concluded that the Hausner ratio was the most precise measurement of powder flowability. Thus, this parameter has been implemented in the dimensionless models (equations 16 and 17), corresponding to the powder flowability characteristic. This will increase the accuracy and the robustness of the model.

In order to fit the dimensionless models to the experimental data, the two models, $\bar{t}$ and p_{CSTR}, were split into two, depending on the filling degree value. Indeed, it has been noticed that, when the filling degree is high enough so that the powder passes over the shaft, the hydrodynamic is changed (Figure 12). These two hydrodynamics types must be treated separately, with FD_{OF} the limit taken from the dimensionless model from section 3.2.

Table 9: Experimental results from the RTD with $FD<FD_{OF}$

Hausner (-)	FD (%)	Fr (-)	p_{sc}/D_{sc} (-)	$\bar{t}/\tau$ (-)	p_{CSTR} (-)
1.17	19%	$1.97.10^{-6}$	0.47	1.09	0.13
	19%	$1.97.10^{-6}$		1.07	0.11
	19%	$1.97.10^{-6}$		1.04	0.09
	19%	$1.97.10^{-6}$		1.07	0.11
	26%	$1.97.10^{-6}$		1.05	0.09
	10%	$7.88.10^{-6}$		1.13	0.17
	25%	$7.88.10^{-6}$		1.06	0.10
	19%	$1.97.10^{-6}$		1.07	0.11
	11%	$2.91.10^{-7}$		1.16	0.17
	24%	$2.91.10^{-7}$		1.05	0.08
	10%	$1.97.10^{-6}$		1.13	0.14
	31%	$2.02.10^{-6}$	0.30	1.04	0.06
	20%	$2.02.10^{-6}$		1.03	0.04
	6%	$2.02.10^{-6}$		1.06	0.07
	9%	$2.02.10^{-6}$		1.04	0.06
	10%	$2.02.10^{-6}$		1.04	0.07
	12%	$1.17.10^{-6}$		1.07	0.08
	21%	$1.17.10^{-6}$		1.05	0.06
	32%	$1.17.10^{-6}$		1.02	0.04
1.27	10%	$5.14.10^{-6}$	0.47	1.04	0.06
	10%	$2.02.10^{-6}$	0.30	1.01	0.04
	9%	$2.02.10^{-6}$		1.03	0.04
	10%	$1.17.10^{-6}$		1.05	0.04
	34%	$1.17.10^{-6}$		1.01	0.02

1.42	9%	$2.91.10^{-7}$	0.47	1.01	0.03
	9%	$2.91.10^{-7}$		1.02	0.03
	10%	$6.16.10^{-6}$		1.02	0.05
	10%	$2.02.10^{-6}$	0.30	1.01	0.02
	10%	$2.02.10^{-6}$		1.00	0.02
	10%	$1.17.10^{-6}$		1.03	0.03
	31%	$1.17.10^{-6}$		1.02	0.03

Table 10: Experimental results from the RTD with FD>FD_{OF}

Hausner (-)	FD (%)	Fr (-)	p_{sc}/D_{sc} (-)	$\bar{t}/\tau$ (-)	p_{CSTR} (-)
1.17	26%	$1.97.10^{-6}$	0.47	1,05	0,09
	25%	$7.88.10^{-6}$		1,06	0,10
	24%	$2.91.10^{-7}$		1,05	0,08
	41%	$4.21.10^{-6}$		1,16	0,11
	41%	$2.91.10^{-7}$		1,20	0,08
	40%	$8.09.10^{-6}$	0.30	1,10	0,09
	40%	$8.09.10^{-6}$		1,06	0,09
	31%	$2.02.10^{-6}$		1,04	0,06
	32%	$1.17.10^{-6}$		1,02	0,04
1.27	41%	$5.14.10^{-6}$	0.47	1,08	0,08
	39%	$2.02.10^{-6}$	0.30	1,03	0,05
	39%	$2.02.10^{-6}$		1,04	0,04
	43%	$1.17.10^{-6}$		1,15	0,04
	34%	$1.17.10^{-6}$		1,01	0,02
1.42	37%	$6.16.10^{-6}$	0.47	1,07	0,07
	36%	$2.91.10^{-7}$		1,08	0,07
	36%	$2.02.10^{-6}$	0.30	1,02	0,02
	36%	$2.02.10^{-6}$		1,00	0,02
	42%	$1.17.10^{-6}$		1,04	0,04
	31%	$1.17.10^{-6}$		1,02	0,03

Therefore, the models were fitted for FD≤ FD_{OF}, representing 31 experimental data (Table 9), and for FD≥ FD_{OF}, representing 20 experimental data (Table 10). The parameters with their standard deviation for the predicted mean residence time and p_{CSTR} for $FD \leq FD_{OF}$ are listed in Table 11 while for those with $FD \geq FD_{OF}$ are listed in Table 12. Using parameters from Table 11 or Table 12 depends if FD is lower or higher than FD_{OF}. FD_{OF} is calculated with equation 13 and with the parameter from Table 4.

Table 11: Parameters and their standard deviation for the mean residence time prediction (equation 16) and CSTR volume proportion (equation 17), without overflow ($FD \leq FD_{OF}$)

$\bar{t}$ prediction			p_{CSTR} prediction		
Parameter	Value	Standard deviation	Parameter	Value	Standard deviation
k	1.087	0.082	k’	0.565	0.256
α	-0.023	0.010	α'	-0.472	0.078
β	-0.003	0.005	β’	-0.006	0.030
γ	-0.293	0.061	γ'	-7.578	0.903
δ	0.065	0.020	δ’	1.748	0.182

Table 12: Parameters and their standard deviation for the mean residence time prediction (equation 16) and CSTR volume proportion (equation 17), with overflow ($FD \geq FD_{OF}$)

$\bar{t}$ prediction			p_{CSTR} prediction		
Parameter	Value	Standard deviation	Parameter	Value	Standard deviation
k	1.398	0.123	k’	2.366	1.471
α	0.203	0.035	α'	0.313	0.223
β	-0.010	0.006	β’	0.115	0.039
γ	-0.291	0.075	γ'	-2.980	0.707
δ	0.121	0.027	δ’	1.160	0.216

First, it can be seen that the Froude coefficient, noted β and β′ in Table 11 and Table 12, is negligible compared to other coefficients, which is in agreement with Figure 12. Regarding the filling degree, if $FD \leq FD_{OF}$, increasing this parameter reduces the mean residence time and the volume proportion of continuous stirred tank, but inversely when $FD \geq FD_{OF}$. This is in agreement with Waje *et al.* when describing the different flow behaviour regarding of the filling degree [2,4] and with the conclusion from section 3.2. Moreover, when increasing the Hausner ratio, the mean residence time is reduced, in agreement with section 3.5. Finally, lengthening the pitch increases the mean residence time, which is in agreement with Figure 14.

The parity plots are presented on Figure 15. It can be seen that the mean residence times predicted are really close to the experimental values. Regarding the p_{CSTR} proportion, some deviations may appear, but most of these values are in between the 20% error margin. In any case, the RTD can be accurately predicted with these four models, even if the powder flows below or above the shaft.

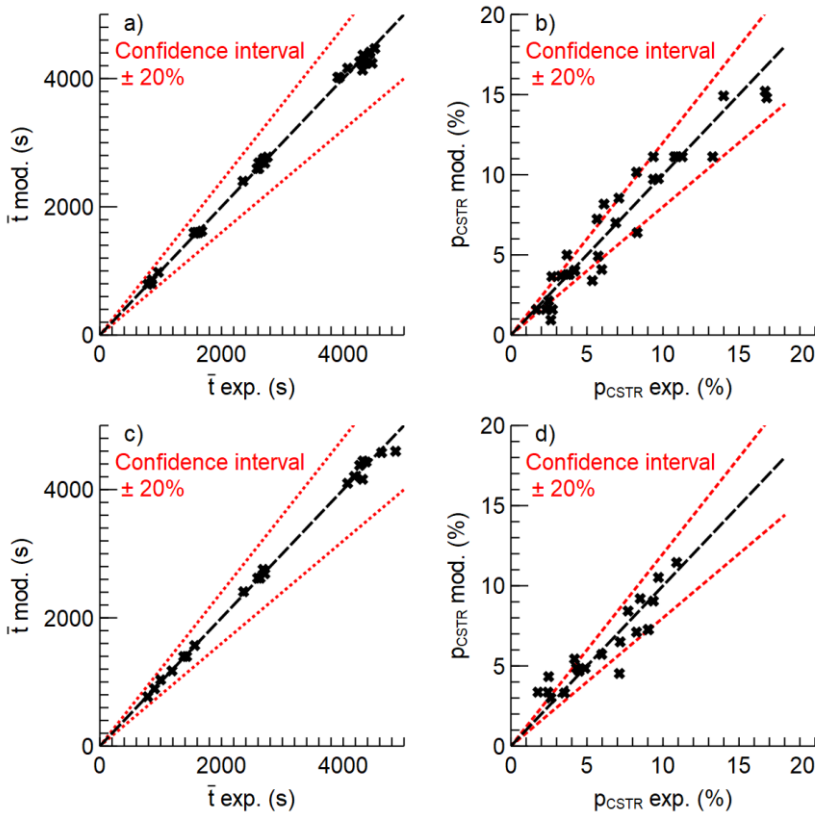

Figure 15: Parity plot for the mean residence time and p_{CSTR} proportion: a) and b) for $FD \leq FD_{OF}$ with equations 16 and 17 using parameters from Table 11 and c) and d) for $FD \geq FD_{OF}$ with equations 16 and 17 using parameters from Table 12

3.8. Comparison of the model with literature experimental data

Many RTD measurements can be found in the literature for screw conveyors. The dimensionless model presented in section 3.7 will be compared with experimental data found by other authors. The operating conditions are described in Table 13. The Hausner ratio for Huo *et al.* was set to Waje's *et al.* value, as the authors did not specify this parameter. The wood chip Hausner ratio value for Chamberlin *et al.* was taken from [43]. The value for Nachenius *et al.* regarding the rice was taken from [39,41], the other values were taken equal to Waje and Chamberlin, as no Hausner ratio value was available.

Table 13: Operating condition and screw geometry for RTD comparison

Authors	Operating condition and geometry			
Waje *et al.* [2]	$0.01 < FD < 0.14$	$2.38 \times 10^{-4} < Fr < 1.60 \times 10^{-3}$	HR=1.15 (sand)	$\frac{p_{sc}}{D_{sc}} = 1.8$
Huo *et al.* [44]	$0.15 < FD < 0.16$	$2.02 \times 10^{-5} < Fr < 3.24 \times 10^{-4}$	HR=1.15 (sand)	$\frac{p_{sc}}{D_{sc}} = 0.4$
Chamberlin *et al.* [34]	$0.05 < FD < 0.13$	$4.10 \times 10^{-6} < Fr < 3.51 \times 10^{-5}$	HR=1.38 (wood chip)	$\frac{p_{sc}}{D_{sc}} = 0.4$
Nachenius *et al.* [24]	$0.05 < FD < 0.13$	$7.46 \times 10^{-5} < Fr < 1.20 \times 10^{-3}$	HR=1.15 (sand) HR=1.38 (pine) HR=1.05 (rice)	$\frac{p_{sc}}{D_{sc}} = 1$
Our study	0.06<FD<0.43	$2.91 \times 10^{-7} < Fr < 8.09 \times 10^{-6}$	1.17<HR<1.42	$0.3<\frac{p_{sc}}{D_{sc}}<0.5$

The parity plot on Figure 16 shows the comparison of mean residence time between literature experimental data and dimensionless model. First, it can be seen that the mean residence time measured by Waje *et al.* [2] is much higher than the mean residence time predicted. In their study, Waje *et al.* pointed out that the mean residence time is about 3 times higher than the reactor residence time, which is far from our results. It is rather strange to find such ratio, as the reactor hydrodynamic is close to a plug flow reactor. Yet, their screw reactor was in a U-trough shape, giving a varying gap between the screw and the reactor wall and probably a different hydrodynamic pattern.

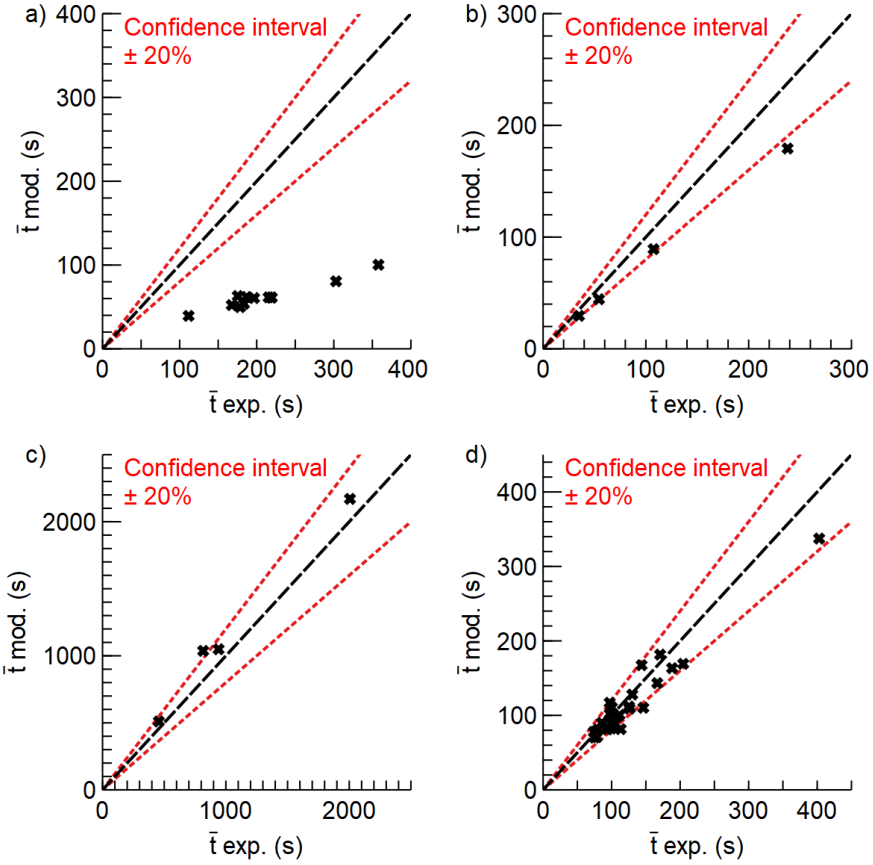

Figure 16: Comparison of mean residence time between literature experimental data and the dimensionless model from equation 16 using parameters from Table 11 and Table 12 : a) Waje *et al.* [2], b) Huo *et al.* [44], c) Chamberlin *et al.* [34] and d) Nachenius *et al.* [24]

Regarding the other studies, the dimensionless model predicts with good accuracy the mean residence time, even if the solid properties or the screw geometries are very different from the experimental condition used to develop the model. Indeed, the other authors studied large particle diameter (between 0.1 and 1 mm), with a particle diameter D_{90} to clearance ratio between 0.2 and 1. In our study, this ratio was around 0.1. Moreover, the study from Nachenius *et al.* is with a pitch length equal to the screw diameter, which is approximately twice of our ratio. This shows that the dimensionless model could be used to predict the mean residence time for a wide range of conditions. Unfortunately, it was not possible to compare the p_{CSTR} value predicted with the dimensionless model and with literature experimental data, as no such model was used to model the RTD in a screw conveyor reactor.

4. CONCLUSION

Hydrodynamic of powder in a screw conveyor has been studied using the Residence Time Distribution (RTD). Two different methods to characterise the powder hydrodynamics and two

models to represent the RTD have been compared. A dimensionless model, using the Vashy-Buckingham theorem, has been developed and fitted with 51 experimental data.

The Hausner ratio has been chosen as the powder flowability property. Although the static angle of repose is a known flowability parameter, the Hausner ratio gave the less relative standard deviation when measuring this parameter (around 4%). Therefore, it should be more accurate to use this parameter in the dimensionless model.

The overflow point, noted $\mathrm{FD_{OF}}$ and described as the filling degree value when the powder started to flow over the shaft, was determined for different rotation speeds, powder flowability and screw geometries. The pitch length was the most influential parameter. A dimensionless model was fitted with 21 experimental data, which predicts with good accuracy the overflow point. The parameters are listed in Table 4.

The flow rate variation to study the transitional state showed that it was not applicable in our case, as the hydrodynamic was completely disturbed during the variation. Although the curve was not treated, the results showed that the screw reactor stabilised quickly, up to 1.3 times the conveyor time of passage for good flowability powder. Moreover, it suggested that the filling degree has an effect on the flow behaviour. Finally, the powder contained in pitch does exchange with the previous one, but not with the next one.

The injection of salty powder was used to study the RTD. The method was confirmed by comparing some repeatable experiments. The RTD curves are characterised by a long delay (equal to the conveyor time of passage), a huge peak and an exponential decrease. Such results can be found in the literature. Thus, the RTD curve can either be described with a gamma distribution model or with a compartment model. As the RTD is asymmetrical, three parameters were needed to fit the gamma distribution while only two parameters are required for the compartment model. Indeed, a Plug Flow Reactor (PFR) in series with a Continuous Stirred Tank Reactor (CSTR) represents with accuracy the RTD results. This compartment model either need the PFR volume proportion ($\mathrm{p_{PFR}}$) or the CSTR volume proportion ($\mathrm{p_{CSTR}}$), and the mean residence time. Therefore, the dimensionless model was constructed in order to predict the mean residence time and $\mathrm{p_{CSTR}}$.

The operating and the geometric parameters were varied to see any influence on the RTD. First, it appears that in a screw reactor, two different hydrodynamics can be found in a screw, depending on the filling degree (FD). Indeed, when FD$\geq \mathrm{FD_{OF}}$, the powder passes over the shaft, increasing the powder residence time in the screw conveyor. Secondly, the Froude number, the screw length and the reactor wall material had no significant effect on the RTD. Finally, the Hausner ratio (powder flowability) and the pitch length modified the RTD shape. Increasing the Hausner ratio (decreasing the powder flowability) and reducing the pitch length narrow the RTD curve, reducing the global mixing.

The two dimensionless models were fitted on the experimental data. As the hydrodynamics are completely changed when the powder passes over the shaft, the two parameters models were split into four models. Two were fitted with 31 experimental data having FD$\leq \mathrm{FD_{OF}}$ and two were fitted with 20 experimental data having FD$\geq \mathrm{FD_{OF}}$. In each case, the two models predict accurately our RTD results. The parameters are listed in Table 11 and Table 12. This model also demonstrates good accuracy by predicting other literature experimental data. Such tool can be used to predict the hydrodynamic when scaling up a screw reactor involving powder conveying.

In a screw reactor, the prediction of the reaction can be difficult, especially with complex reaction. Thus, using dimensionless models that predict the global mixing for any operating conditions or geometric device can be helpful. Such tools can be used when designing a screw reactor, even at a plant scale.

APPENDIX: UNCERTAINTY CALCULATIONS FOR E(T)

The uncertainty of a function f as $f = \frac{a}{b}$ is calculated as

$$\frac{\delta f}{f} = \frac{\delta a}{a} + \frac{\delta b}{b}$$

Thus, for the E(t) function, the uncertainty $\delta E(t)$ can be calculated as follows

$$E(t) \approx \frac{c_{pulse}(t_i)}{\sum_{i=0}^{Ns} c_{pulse}(t_i)\Delta t_i}$$

$$\delta \mathrm{E(t)} = \mathrm{E(t)}.\left(\frac{\delta \mathrm{c_{pulse}(t_i)}}{\Delta \mathrm{c_{pulse}(t_i)}} + \frac{\delta \sum_{i=0}^{Ns} c_{pulse}(t_i)\Delta t_i}{\sum_{i=0}^{Ns} c_{pulse}(t_i)\Delta t_i}\right)$$

$$\delta \sum_{i=0}^{Ns} c_{pulse}(t_i)\Delta t_i = \sum_{i=0}^{Ns} c_{pulse}(t_i)\Delta t_i \left(\frac{\delta c_{pulse}(t_i)}{c_{pulse}(t_i)} + \frac{\delta \Delta t_i}{\Delta t_i}\right)$$

$$\delta \mathrm{E(t)} = \mathrm{E(t)}.\left(\frac{\delta \mathrm{c_{pulse}(t_i)}}{\Delta \mathrm{c_{pulse}(t_i)}} + \frac{\sum_{i=0}^{Ns} c_{pulse}(t_i)\Delta t_i \left(\frac{\delta c_{pulse}(t_i)}{c_{pulse}(t_i)} + \frac{\delta \Delta t_i}{\Delta t_i}\right)}{\sum_{i=0}^{Ns} c_{pulse}(t_i)\Delta t_i}\right)$$

REFERENCES

[1] A.S. Mujumdar, Book Review: Handbook of Industrial Drying, Third Edition, Dry. Technol. 25 (2007) 1133–1134. https://doi.org/10.1080/07373930701399224.

[2] S.S. Waje, A.K. Patel, B.N. Thorat, A.S. Mujumdar, Study of residence time distribution in a pilot-Scale screw conveyor dryer, Dry. Technol. 25 (2007) 249–259. https://doi.org/10.1080/07373930601161120.

[3] F. Campuzano, R.C. Brown, J.D. Martínez, Auger reactors for pyrolysis of biomass and wastes, Renew. Sustain. Energy Rev. 102 (2019) 372–409. https://doi.org/10.1016/j.rser.2018.12.014.

[4] S.S. Waje, B.N. Thorat, A.S. Mujumdar, Hydrodynamic Characteristics of a Pilot-Scale Screw Conveyor Dryer, Dry. Technol. 25 (2007) 609–616. https://doi.org/10.1080/07373930701250120.

[5] S.S. Waje, B.N. Thorat, A.S. Mujumdar, An experimental study of the thermal performance of a screw conveyor dryer, Dry. Technol. 24 (2006) 293–301. https://doi.org/10.1080/07373930600564506.

[6] S.S. Waje, B.N. Thorat, A.S. Mujumdar, Screw Conveyor Dryer: Process and Equipment Design, Dry. Technol. 25 (2007) 241–247. https://doi.org/10.1080/07373930601161112.

[7] F. Codignole Luz, S. Cordiner, A. Manni, V. Mulone, V. Rocco, Biomass fast pyrolysis in screw reactors: Prediction of spent coffee grounds bio-oil production through a monodimensional model, Energy Convers. Manag. 168 (2018) 98–106. https://doi.org/10.1016/j.enconman.2018.04.104.

[8] R.W. Nachenius, J.H.A.J. Kiel, W. Prins, Torrefaction: Upgrading biomass into high-quality solid bioenergy carriers, Biomass Power World Transform. to Eff. Use. 0 (2015) 395–424. https://doi.org/10.1201/b18314-15.

[9] R.W. Nachenius, T.A. van de Wardt, F. Ronsse, W. Prins, Torrefaction of pine in a bench-scale screw conveyor reactor, Biomass and Bioenergy. 79 (2014) 96–104. https://doi.org/10.1016/j.biombioe.2015.03.027.

[10] F. Codignole Luz, S. Cordiner, A. Manni, V. Mulone, V. Rocco, Biomass fast pyrolysis in a shaftless screw reactor: A 1-D numerical model, Energy. 157 (2018) 792–805. https://doi.org/10.1016/j.energy.2018.05.166.

[11] D.A. Sievers, J.J. Stickel, Modeling residence-time distribution in horizontal screw hydrolysis reactors, Chem. Eng. Sci. 175 (2018) 396–404. https://doi.org/10.1016/j.ces.2017.10.012.

[12] O. Kaplan, C. Celik, Woodchip drying in a screw conveyor dryer, J. Renew. Sustain. Energy. 4 (2012). https://doi.org/10.1063/1.4766890.

[13] Y. Yu, P.C. Arnold, Theoretical modelling of torque requirements for single screw feeders, Powder Technol. 93 (1997) 151–162. https://doi.org/10.1016/S0032-5910(97)03265-8.

[14] J. Dai, J.R. Grace, A model for biomass screw feeding, Powder Technol. 186 (2008) 40–55. https://doi.org/10.1016/j.powtec.2007.10.032.

[15] T. UEMATU, S. NAKAMURA, A Study of the Screw Conveyor, Bull. JSME. 3 (1960) 449–455. https://doi.org/10.1299/jsme1958.3.449.

[16] J.R. Metcalf, The Mechanics of the Screw Feeder, Proc. Inst. Mech. Eng. 180 (1965) 131–146. https://doi.org/10.1243/PIME_PROC_1965_180_015_02.

[17] A.W. Roberts, The influence of granular vortex motion on the volumetric performance of enclosed screw conveyors, Powder Technol. 104 (1999) 56–67. https://doi.org/10.1016/S0032-5910(99)00039-X.

[18] D. Minglani, A. Sharma, H. Pandey, R. Dayal, J.B. Joshi, S. Subramaniam, A review of granular flow in screw feeders and conveyors, Powder Technol. 366 (2020) 369–381. https://doi.org/10.1016/j.powtec.2020.02.066.

[19] A.J. Carleton, J.E.P. Miles, F.H.H. Valentin, A study of factors affecting the performance of screw conveyers and feeders, J. Manuf. Sci. Eng. Trans. ASME. 91 (1969) 329–333.

https://doi.org/10.1115/1.3591565.
[20] D. Mondal, Nabendughosh, Study on filling factor of short length screw conveyor with flood-feeding condition, Mater. Today Proc. 5 (2018) 1286–1291. https://doi.org/10.1016/j.matpr.2017.11.213.
[21] X. Li, Q. Hou, K. Dong, R. Zou, A. Yu, Promote cohesive solid flow in a screw feeder with new screw designs, Powder Technol. 361 (2020) 248–257. https://doi.org/10.1016/j.powtec.2019.08.045.
[22] F.J.C. Rademacher, Some aspects of the characteristics of vertical screw conveyors for granular material, Powder Technol. 9 (1974) 71–89. https://doi.org/10.1016/0032-5910(74)85011-4.
[23] F.J.C. Rademacher, On seed damage in grain augers, J. Agric. Eng. Res. 26 (1981) 87–96. https://doi.org/10.1016/0021-8634(81)90129-3.
[24] R.W. Nachenius, T.A. Van De Wardt, F. Ronsse, W. Prins, Residence time distributions of coarse biomass particles in a screw conveyor reactor, Fuel Process. Technol. 130 (2015) 87–95. https://doi.org/10.1016/j.fuproc.2014.09.039.
[25] L. Pezo, A. Jovanović, M. Pezo, R. Čolović, B. Lončar, Modified screw conveyor-mixers - Discrete element modeling approach, Adv. Powder Technol. 26 (2015) 1391–1399. https://doi.org/10.1016/j.apt.2015.07.016.
[26] A.W. Roberts, A.H. Willis, Performance of Grain Augers, Proc. Inst. Mech. Eng. 176 (1962) 165–194. https://doi.org/10.1243/PIME_PROC_1962_176_021_02.
[27] G. E. Rehkugler and L. L. Boyd, Dimensional Analysis of Auger Conveyor Operation, Trans. ASAE. 5 (1962) 0098–0102. https://doi.org/10.13031/2013.40945.
[28] D.A. Sievers, E.M. Kuhn, J.J. Stickel, M.P. Tucker, E.J. Wolfrum, Online residence time distribution measurement of thermochemical biomass pretreatment reactors, Chem. Eng. Sci. 140 (2016) 330–336. https://doi.org/10.1016/j.ces.2015.10.031.
[29] P.J. Owen, P.W. Cleary, Prediction of screw conveyor performance using the Discrete Element Method (DEM), Powder Technol. 193 (2009) 274–288. https://doi.org/10.1016/j.powtec.2009.03.012.
[30] H.M. Beakawi Al-Hashemi, O.S. Baghabra Al-Amoudi, A review on the angle of repose of granular materials, Powder Technol. 330 (2018) 397–417. https://doi.org/10.1016/j.powtec.2018.02.003.
[31] M. Sebastian Escotet-Espinoza, S. Moghtadernejad, S. Oka, Y. Wang, A. Roman-Ospino, E. Schäfer, P. Cappuyns, I. Van Assche, M. Futran, M. Ierapetritou, F. Muzzio, Effect of tracer material properties on the residence time distribution (RTD) of continuous powder blending operations. Part I of II: Experimental evaluation, Powder Technol. 342 (2019) 744–763. https://doi.org/10.1016/j.powtec.2018.10.040.
[32] L.G. Hernández, J.G. Pérez, M. Gaytán-Martínez, Tracers used in granular systems: Review, Powder Technol. 340 (2018) 274–289. https://doi.org/10.1016/j.powtec.2018.09.025.
[33] K. Saleh, S. Golshan, R. Zarghami, A review on gravity flow of free-flowing granular solids in silos – Basics and practical aspects, Chem. Eng. Sci. 192 (2018) 1011–1035. https://doi.org/10.1016/j.ces.2018.08.028.
[34] C. Chamberlin, D. Carter, A. Jacobson, Measuring residence time distributions of wood chips in a screw conveyor reactor, Fuel Process. Technol. 178 (2018) 271–282. https://doi.org/10.1016/j.fuproc.2018.06.005.
[35] O. Levenspiel, Tracer Technology, Springer New York, New York, NY, 2012. https://doi.org/10.1007/978-1-4419-8074-8.
[36] K. Lachin, Z. Youssef, G. Almeida, P. Perré, D. Flick, Residence time distribution analysis in the transport and compressing screws of a biomass pretreatment process, Chem. Eng. Res. Des. 154 (2020) 162–170. https://doi.org/10.1016/j.cherd.2019.12.011.
[37] T.A. Kingston, T.A. Geick, T.R. Robinson, T.J. Heindel, Characterizing 3D granular flow structures in a double screw mixer using X-ray particle tracking velocimetry, Powder Technol. 278 (2015) 211–222. https://doi.org/10.1016/j.powtec.2015.02.061.
[38] D. Minglani, A. Sharma, H. Pandey, R. Dayal, J.B. Joshi, Analysis of flow behavior of

size distributed spherical particles in screw feeder, Powder Technol. 382 (2021) 1–22. https://doi.org/10.1016/j.powtec.2020.12.041.
[39] A.S. Bongo Njeng, S. Vitu, M. Clausse, J.L. Dirion, M. Debacq, Effect of lifter shape and operating parameters on the flow of materials in a pilot rotary kiln: Part I. Experimental RTD and axial dispersion study, Powder Technol. 269 (2015) 554–565. https://doi.org/10.1016/j.powtec.2014.03.066.
[40] F. Qi, T.J. Heindel, M.M. Wright, Numerical study of particle mixing in a lab-scale screw mixer using the discrete element method, Powder Technol. 308 (2017) 334–345. https://doi.org/10.1016/j.powtec.2016.12.043.
[41] A.S. Bongo Njeng, S. Vitu, M. Clausse, J.L. Dirion, M. Debacq, Effect of lifter shape and operating parameters on the flow of materials in a pilot rotary kiln: Part II. Experimental hold-up and mean residence time modeling, Powder Technol. 269 (2015) 566–576. https://doi.org/10.1016/j.powtec.2014.05.070.
[42] M. Meise, L. Jäger, A. Wilk, T. Heitmann, S. Scholl, Residence Time Characteristics of the Novel Archimedean Screw Crystallizer/Reactor, Chemie-Ingenieur-Technik. 92 (2020) 1074–1082. https://doi.org/10.1002/cite.202000092.
[43] H. Salehi, M. Poletto, D. Barletta, S.H. Larsson, Predicting the silo discharge behavior of wood chips - A choice of method, Biomass and Bioenergy. 120 (2019) 211–218. https://doi.org/10.1016/j.biombioe.2018.11.023.
[44] C. Huo, C. Fan, P. Feng, W. Lin, W. Song, Residence Time Distribution of Particles in a Screw Feeder: Experimental and Modelling Study, Can. J. Chem. Eng. 93 (2015) 1635–1642. https://doi.org/10.1002/cjce.22240.